Low-Cost Parameter Estimation Approach for Modular Converters and Reconfigurable Battery Systems Using Dual Kalman Filter

N. Tashakor, *Student Member, IEEE*, B. Arabsalmanabadi, *Student Member, IEEE*, F. Naseri, and S. Goetz, *Member, IEEE*

***Abstract*—Modular converters or reconfigurable battery energy storage systems are a promising approach to eliminate the dependence on the weakest element in previously hard-wired battery packs and to combine heterogeneous batteries (so-called mixed-battery systems). But their need for expensive sensors and complex monitoring as well as control subsystems hinders their progress. Estimating parameters of each module can substantially reduce the number of required sensors and/or communication components. However, the existing estimation methods for cascaded modular circuits neglect important parameters such as the internal resistance of the battery, resulting in large systematic errors and bias. This paper proposes an online estimator based on a dual-Kalman filter (DKF) that exploits the slow dynamics of the battery compared to the load. The DKF algorithm estimates the open-circuit voltage (OCV) and internal resistance of each module by measuring only the output voltage and current of the system. Compared with the state of the art, the proposed method is simpler and cheaper with only two sensors compared to ≥ N + 2 (*N* is the number of modules). Furthermore, the proposed algorithm achieves a fast convergence through optimal learning rate. Simulations and experimental results confirm the ability of the proposed approach, achieving < 1.5% and < 5% estimation error for OCV and the internal resistance, respectively.**

***Index Terms*—Modular multilevel converter (MMC), reconfigurable battery, split battery, dual Kalman filter (DKF), parameter estimation, cascaded bridge converter.**

I. Introduction

MODULAR multilevel converters (MMC) and cascaded half-bridges (CHB) dominate high-voltage applications due to flexibility and cost-effective expandability [5]. However, with the falling price of power electronics, popularity of MMCs and/or CHBs is also growing in medium- and low-voltage applications [6, 7]. One major trend is integration with considerably large battery energy storages resulting in a fully controlled modular converter/battery pack [10, 11]. This also allows a flexible connection of multiple strings to form different dc, single-phase, and multi-phase structures [12, 13].

On the module level, modular converters can use different topologies, among which the half-bridge (HB) topology is the most popular one at the moment [15, 16]. Two switches within each module form the simplest circuit and lowest cost among several configurations [17-19]. Although integration of batteries in a modular converter offers many advantages including higher fault tolerance and more degrees of freedom, it still necessitates a variety of functions for monitoring, balancing, and protection of these systems. To ensure battery safety, continuous monitoring of state variables is an unquestionable necessity [22, 23]. Moreover, the inherent parameter spread of the module components and different environmental conditions as well as different aging factors can lead to charge imbalance across the modules and reduced system performance [24-26]. Therefore, the modules must be constantly monitored to ensure balanced, stable, and safe operation of the system [27].

Although parameter estimation techniques for battery packs are extensively studied, almost all of them consider the battery pack as a whole, which makes them incompatible with dynamically reconfigurable batteries [20, 28, 29]. It may be possible to modify many of those techniques for module-level application in combination with real-time measurements of the modules' parameters. However, in a high-power industrial application with hundreds of modules, the collection, transmission, and processing of all these data is a significant challenge and from a cost-perspective inacceptable. Numerous sensors increase the cost and size of the data acquisition system beyond manageable levels. Particularly current sensors are critical as they have to be rated for the entire load current. For example, for a system with N modules, there can be up to $(2N + 2)$ isolated voltage and current sensors.

A similar challenge exists for monitoring the states and parameters of the modules in MMCs and CHBs. Recent scientific works investigate the reduction of direct measurement at the module level for modules with capacitors by incorporating state observers to estimate their voltage [3, 4]. The implemented methods vary from recursive techniques such as least-square [1] and model-based estimators such as Kalman filters [31, 33] to methods using machine learning [8]. Konstantinou et al. review different estimation/observation methods for monitoring voltage of each module in an MMC [35].

Most of the reported techniques for capacitor-based modules are to some degree applicable for estimating the terminal voltage of the batteries [3]. However, whereas the internal resistance of the capacitors is negligible, the internal resistance of the batteries is considerably higher and cannot be neglected [32]. Furthermore, the internal resistance of a battery is a crucial indicator for determining age, and it is a key to perform fault prognosis [20, 32]. Finally, although the terminal voltage of the battery is a particularly good indicator of its charge after a long idle period, the

terminal voltage of a battery under load/charge can significantly vary from its open-circuit value [36, 37].

Therefore, even though a wide range of techniques is available for estimating terminal voltages of the modules in MMCs, none of them is capable of accurately estimating the internal resistance and the open-circuit voltage of the modules [20, 37, 38]. Model-free estimators that estimate the resistance and voltage of a modular battery based on particle swarm optimization (PSO) through continuous optimization of the squared errors are previously presented [30, 39]. However, since it is based on PSO, it requires heavy computation and has considerably slower convergence speed or accuracy. Another significant difference between modules with capacitors and modules with batteries is their dynamics. The capacitor voltage varies continuously with relatively fast dynamics, requiring high convergence speed and fast update rates. However, the battery parameters enjoy a slower dynamic, which can be leveraged to reduce the estimator complexity and noise susceptibility [40].

Table I provides a general comparison of the state-of-the-art estimation techniques with the proposed method. In short, the available estimation methods for batteries are expensive and demanding, and the available estimation methods with reduced sensors neglect the internal resistance of the batteries.

Simultaneous estimation of both the internal resistance and internal voltage of all the battery modules in a dynamically reconfigurable pack with minimum sensors builds the main contribution of this work, which has not been previously addressed. Instead, other reports consider batteries or capacitors only as a single dc source with a negligible or predetermined fixed internal resistance [33, 40-42] or they require at least two sensors per module ($2N$ sensors for N battery modules), increasing cost and complexity [14, 20, 28, 30, 32].

The open-circuit voltage as well as the resistance of the battery are time-varying parameters that are closely tied to most monitoring and protection functions, e.g., performing balancing and ensuring the operating points of the batteries are within safe regions (to prevent over-charge or over-discharge). [13, 26, 43]. However, deriving an accurate value for the open-circuit voltage under load without knowing the internal resistance of the battery is not possible. Furthermore, previous research shows a direct link between aging and the equivalent resistance of the module, which further adds to the importance of this parameter [20].

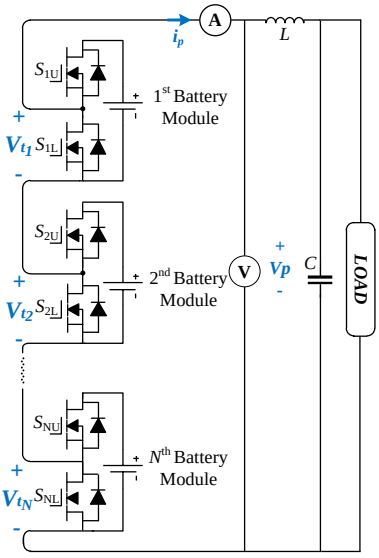

Fig. 1. A single arm battery-based dc MMC/CHB macro structure

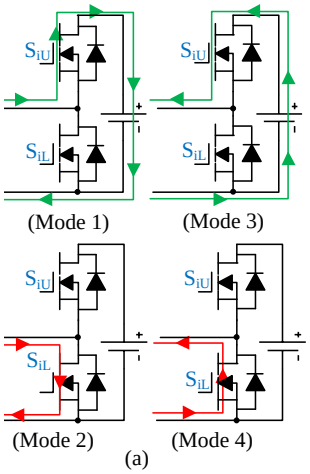

Fig. 2. Different operating mod battery-integrated half-bridge modu

The proposed method decouples the estimation of module-level voltages and resistances through regular sampling of only the voltage and current at the output through a dual-Kalman-filter (DKF) algorithm. Furthermore, the learning factor of the system is optimized to speed up the convergence and improve the dynamic performance. The proposed technique benefits from low computation needs and can be implemented in most low-end controllers, without any additional sensors for the modules.

II. Selected Modular Structure

Fig. 1 depicts the topology of a dynamically reconfigurable battery consisting of N battery-based modules, inductor L, capacitor C, and the load or charger. Only two sensors at the output terminals measure the voltage and current of the system with the sampling time T_s, and no extra sensors are necessary at the module terminals. Each module includes a battery with one or several

TABLE I
General Comparison of the Estimation Techniques

	Method	Estimate	Considers Nonlinearity	Applicable to Modules	Sensor Count	Comments
Methods for MMC parameter estimation	KF for MMCs [1]	V_t [(1)]	no	yes	2	− does not consider capacitor effect; − is affected by sampling delay; − neglects the resistance effect
	Based on two step estimation (model and measurement) [2]	V_t	no	yes	2	− is affected by the sampling delay; − neglects the resistance effect; + relatively simple
	Voltage estimation based on energy variations in the capacitor [3]	V_t	no	yes	2	− affected by sampling delay; − neglects the resistance effect
	Iterative based method with delay compensation [4]	V_t	no	yes	≥ 4	− neglects the resistance effect; − at least two extra sensors; + more stable
	Voltage estimation based on Adaline iterative algorithm [8, 9]	V_t	no	yes	2	− affected by sampling delay; − neglects the resistance effect; − Adaline method convergence speed is lower than KF; − Adaline is simpler than KF
Methods for battery parameter estimation	Extended KF for battery packs [14]	V_{oc}, R_{bt}, τ	yes	no	$2N$	− requires direct measurement at the terminals of the battery; − high number of sensors; − neglects the resistance effect; + low sensitivity to noise
	Battery parameters estimation using Gaussian Kernels [20]	SOC, SOH	yes	no	$2N$	− complex; − high number of sensors
	Parameter identification based on the voltage profile [21]	V_{oc}, R_{bt}, τ	yes	no	$2N$	− needs two sensors per battery module; − neglects temperature and SOC effect; + good accuracy
	Parameter identification using PSO [28]	V_{oc}, R_{bt}, τ	yes	no	$2N$	− computationally demanding; − relatively lower accuracy
	Parameter identification based on PSO for modular batteries [1, 8, 30, 31]	V_{oc}, R_{bt}	yes	no	$2N$	− computationally demanding; − relatively lower accuracy
	Impedance based monitoring [32]	SOC, V_{oc}	yes	yes	$3N$	− requires multifrequency current sources; − complex; − requires high-voltage analog multiplexer; − high number of sensors
	Data-driven battery monitoring approach [34]	SOC	yes	yes	$2N$	− computationally demanding; − requires large training datasets; − unpredictable behavior; + can capture the battery nonlinearities perfectly
proposed		V_{oc}, R_{bt}	yes	yes	2	− does not calculate the τ (future work); + only uses the already available sensors at the terminal output; + considers the resistance effects on the measurements

[(1)] *SOC* and *SOH* denote state of charge and state of health, respectively. Also, V_t denotes the terminal voltage, R_{bt} denotes the internal resistance of the battery, and τ is the time constant.

cells and two field-effect transistors (FET, specifically $S_{i\mathrm{U}}$ and $S_{i\mathrm{L}}$) as well as their body diodes (i.e., $D_{i\mathrm{U}}$ and $D_{i\mathrm{L}}$). The modular system is a multilevel dc/dc bidirectional converter, which behaves as a buck/boost converter during the discharge/charge process. Additionally, in some cases, it is possible to include a very small low-pass LC filter between the battery module and the half-bridge to further reduce the stress on the batteries [44]. From the estimation point of view as well as the provided analysis, both cases (with and without filter) are completely identical, neglecting slightly different dynamic responses. For further details, please see the provided online supplement.

A. Battery-Modules Operating Modes

As Fig. 2 shows, each module contains a half-bridge and a battery with four possible operation modes during bidirectional energy transfer as follows: ① $S_{i\mathrm{U}}$ is on, $S_{i\mathrm{L}}$ is off, and the system is charging. The terminal voltage of the module is $v_{t_i} = V_{\mathrm{oc}_i} - (r_{\mathrm{bt}_i} + r_{\mathrm{dU}_i})i_p$ (see Fig. 2(a), Mode 1); ② $S_{i\mathrm{U}}$ is off, $S_{i\mathrm{L}}$ is on, and the system is charging. The module is bypassed, and the terminal voltage of the module is $v_{t_i} = -r_{dsL_i} i_p$ (see Fig. 2(a), Mode 2); ③ $S_{i\mathrm{U}}$ is on, $S_{i\mathrm{L}}$ is off, and the system is discharging. The terminal voltage of the module is $v_{t_i} = v_{\mathrm{oc}_i} - (r_{\mathrm{bt}_i} + r_{\mathrm{dsU}_i})i_p$ (see Fig. 2(a), Mode 3); ④ $S_{i\mathrm{U}}$ is off, $S_{i\mathrm{L}}$ is on, and the system is discharging. The module is bypassed, and the terminal voltage of the module is $v_{t_i} = -r_{\mathrm{dL}_i} i_p$ (see Fig. 2(a), Mode 4). A similar analysis holds true for the cascaded full-bridge structure.

B. Modulation Techniques of the Modules

Among a variety of modulation techniques proposed for CHBs, phase-shifted carrier (PSC) modulation stands out because of its stable performance during dynamic changes and ease of implementation [17, 45]. Fig. 3 provides an intuitive representation of conventional PSC modulation. Additionally, the intuitive representation of dynamic reconfiguration of a modular battery is provided in the online supplement.

III. Battery Parameters Estimation

Internal resistance and the open-circuit voltage of the battery are important parameters and critical for any battery management functionality [32]. Using a simplified mathematical model, the proposed technique estimates the open-circuit voltages (V_{OC}) and internal resistances (r_{bt}) of each module via measuring only the output voltage and current of the system (i.e., v_{p} and i_{p}). In the following section, the mathematical model of the MMC arm or the reconfigurable pack is derived and used for implementation of the DKF-based estimation algorithm.

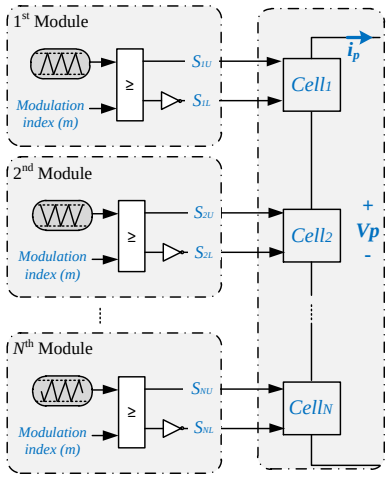

Fig. 3. conventional implementation of the PSC modulation

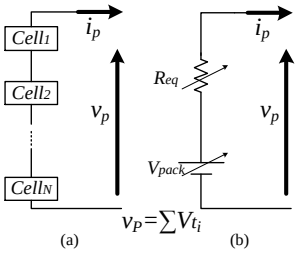

Fig. 4. One arm of an MMC: (a) Converter schematic. (b) Corresponding equivalent circuit

A. Mathematical Model of the MMC

Fig. 4 shows the equivalent electrical circuit of the system shown in Fig. 1. The battery in each module is modeled with a voltage source representing the open-circuit voltage of the battery and an internal series resistance. Although the open-circuit voltage is a function of the battery's state-of-charge (SOC), it can be assumed constant in short estimation intervals for the purpose of modeling. In Fig. 4, R_{eq} is the equivalent resistance of the arm at each instant. Formulating the KVL explicitly for the arm yields

$$v_{\mathrm{p}}^{(t)} = \left(\boldsymbol{S}_{\mathbf{U}}^{(t)}\right)^T \boldsymbol{V}_{\mathbf{OC}} - i_p^{(t)} \left[\left(\boldsymbol{S}_{\mathbf{U}}^{(t)}\right)^T \left(\boldsymbol{R}_{\mathbf{bt}} + \boldsymbol{R}_{\mathbf{ds,U}}\right) + \left(\boldsymbol{S}_{\mathbf{L}}^{(t)}\right)^T \boldsymbol{R}_{\mathbf{d,L}}\right] \tag{2.a}$$

during discharging and

$$v_{\mathrm{p}}^{(t)} = \left(\boldsymbol{S}_{\mathbf{U}}^{(t)}\right)^T \boldsymbol{V}_{\mathbf{OC}} - i_p^{(t)} \left[\left(\boldsymbol{S}_{\mathbf{U}}^{(t)}\right)^T \left(\boldsymbol{R}_{\mathbf{bt}} + \boldsymbol{R}_{\mathbf{d,U}}\right) + \left(\boldsymbol{S}_{\mathbf{L}}^{(t)}\right)^T \boldsymbol{R}_{\mathbf{ds,L}}\right] \tag{2.b}$$

during charging, where $\boldsymbol{S}_{\mathbf{U}}$ is the vector of control signals for the upper switches, $\boldsymbol{S}_{\mathbf{L}}$ is the vector of control signals for the lower ones, $\boldsymbol{R}_{\mathbf{ds}}$ and $\boldsymbol{R}_{\mathbf{d}}$ are the switching resistance and diode resistance vectors, and the subscripts U and L are used to specify upper and lower switches in the half-bridges, respectively. Furthermore, $\boldsymbol{V}_{\mathbf{OC}}$ and $\boldsymbol{R}_{\mathbf{bt}}$ are the vectors of open-circuit voltage and internal resistance of the batteries. $v_p^{(k)}$ and $i_p^{(k)}$ are the measured voltage and current of the output terminal at instant k. Additionally, $\boldsymbol{BA}$ is the cross products of vectors $\boldsymbol{B}$ and $\boldsymbol{A}$. Similarly, $b\boldsymbol{A}$ is the dot product of scalar b and vector $\boldsymbol{A}$.

As shown in Fig. 4, the output current (i_p) is positive during discharging and negative during charging. For simplicity, we assume that the resistances of upper and lower FET switches as well as the resistance of upper and lower diodes are equal, i.e., $\boldsymbol{R}_{\mathbf{ds,U}} = \boldsymbol{R}_{\mathbf{ds,L}} = \boldsymbol{R}_{\mathbf{d,U}} = \boldsymbol{R}_{\mathbf{d,L}} = \boldsymbol{R}_{\mathbf{sw}}$. This assumption is without any loss of generalization, since it is also possible to derive all the following equations considering different resistances for each switch and diode as well as different internal resistances for the batteries during charge or discharge. Applying this simplification, we can rewrite (2) in the discrete domain as

$$v_{\mathrm{p}}^{(k)} = \boldsymbol{S}_{\mathbf{U}}^{(k)} \boldsymbol{V}_{\mathbf{oc}} - i_{\mathrm{p}}^{(k)} \left[\left(\boldsymbol{S}_{\mathbf{U}}^{(k)}\right)^T \boldsymbol{R}_{\mathbf{bt}} + \left(\boldsymbol{S}_{\mathbf{U}}^{(k)} + \boldsymbol{S}_{\mathbf{L}}^{(k)}\right)^T \boldsymbol{R}_{\mathbf{sw}}\right], \tag{3}$$

where subscript k shows the k^{th} sample. Furthermore, since $\boldsymbol{S}_{\mathbf{U}}^{(k)}$ and $\boldsymbol{S}_{\mathbf{L}}^{(k)}$ are complementary, the resultant vector of $\boldsymbol{S}_{\mathbf{U}}^{(k)} + \boldsymbol{S}_{\mathbf{L}}^{(k)}$ is a unity vector. Hence, (3) can be further simplified as

$$v_{\mathrm{p}}^{(k)} = \boldsymbol{S}_{\mathbf{U}}^{(k)} \boldsymbol{V}_{\mathbf{oc}} - i_{\mathrm{p}}^{(k)} \left[\left(\boldsymbol{S}_{\mathbf{U}}^{(k)}\right)^T \boldsymbol{R}_{\mathbf{bt}} + N r_{\mathrm{sw}}\right], \tag{4}$$

where r_{sw} is the internal resistance of one switch or diode and N is the total number of modules.

Obviously, both $\boldsymbol{R}_{\mathbf{bt}}$ and $\boldsymbol{V}_{\mathbf{oc}}$ can affect the output of the system. Therefore, it is necessary to decouple the effect of these two vectors in (4). With that goal in mind, we reformulate (4) for two consecutive instances of k and $(k+1)$ as follows:

$$v_{\mathrm{p}}^{(k)} + i_{\mathrm{p}}^{(k)} N r_{\mathrm{sw}} = \left(\boldsymbol{S}_{\mathbf{U}}^{(k)}\right)^T \boldsymbol{V}_{\mathbf{oc}} - i_{\mathrm{p}}^{(k)} \left(\boldsymbol{S}_{\mathbf{U}}^{(k)}\right)^T \boldsymbol{R}_{\mathbf{bt}}, \tag{5}$$

$$v_{\mathrm{p}}^{(k+1)} + i_{\mathrm{p}}^{(k+1)} N r_{\mathrm{sw}} = \left(\boldsymbol{S}_{\mathbf{U}}^{(k+1)}\right)^T \boldsymbol{V}_{\mathbf{oc}} - i_{\mathrm{p}}^{(k+1)} \left(\boldsymbol{S}_{\mathbf{U}}^{(k+1)}\right)^T \boldsymbol{R}_{\mathbf{bt}}, \tag{6}$$

where k and $(k+1)$ denote two consecutive samples. Subtracting (5) from (6) when $\boldsymbol{S}_{\mathbf{U}}^{(k)} = \boldsymbol{S}_{\mathbf{U}}^{(k+1)} = \boldsymbol{S}_{\mathbf{U}}$, we can remove V_{oc} from the new equations per

$$\Delta v_{\mathrm{p}} + \Delta i_{\mathrm{p}} N r_{\mathrm{sw}} = -\Delta i_{\mathrm{p}} (\boldsymbol{S}_{\mathbf{U}})^T \boldsymbol{R}_{\mathbf{bt}}\,, \tag{7}$$

where $\Delta v_{\mathrm{p}} = v_{\mathrm{p}}^{(k+1)} - v_{\mathrm{p}}^{(k)}$ and $\Delta i_{\mathrm{p}} = i_{\mathrm{p}}^{(k+1)} - i_{\mathrm{p}}^{(k)}$. With $\boldsymbol{R}_{\mathbf{bt}}$ as the only variable, we can rewrite (7) as

$$-\frac{\Delta v_{\mathrm{p}}}{\Delta i_{\mathrm{p}}} - N r_{\mathrm{sw}} = (\boldsymbol{S}_{\mathbf{U}})^T \boldsymbol{R}_{\mathbf{bt}}. \tag{8}$$

With $\boldsymbol{R}_{\mathbf{bt}}$ as the only unknown variable in (8), we can use a KF to update our estimation of the internal resistance of the batteries. After updating our estimation for $\boldsymbol{R}_{\mathbf{bt}}$, another KF will update our estimation of $\boldsymbol{V}_{\mathbf{oc}}$ in (4).

B. DKF Estimator

The DKF estimates the voltage and resistance of each module. Table II provides the implemented pseudo-code of the DKF estimator. Additionally, the flowchart of the proposed technique is provided in the online supplement. At each stage, new measurement samples are acquired to subsequently evaluate the conditions for updating either $\boldsymbol{R}_{\mathbf{bt}}$ or $\boldsymbol{V}_{\mathbf{oc}}$. Assuming k to be the most recent sample, (9) can be written as

$$V_2 = v_{\mathrm{p}}^{(k)},\ I_2 = I_{\mathrm{p}}^{(k)}. \tag{9}$$

Considering a sampling window with w_1 samples and sampling delay of $\tau_s = w_1 T_s$, starting with the first sample in the window and moving toward the oldest one, we can write

$$V_1 = v_{\mathrm{p}}^{(i)}, I_1 = i_{\mathrm{p}}^{(i)}, \tag{10}$$

where i is the first sample in w_1 window by which condition $\boldsymbol{S}_{\mathbf{U}}^{(k)} = \boldsymbol{S}_{\mathbf{U}}^{(i)}$ and $\boldsymbol{S}_{\mathbf{L}}^{(k)} = \boldsymbol{S}_{\mathbf{L}}^{(i)}$ is satisfied. Normally, $\boldsymbol{S}_{\mathbf{U}}^{(k)}$ and $\boldsymbol{S}_{\mathbf{L}}^{(k)}$ are complementary in a half-bridge topology and checking either of the switch vectors can suffice. However, this might not be the case for full-bridge modules or modules with protective circuits.

In the next step, the operation condition of the batteries is determined. To do that, first, the estimator checks the current stability of the $(k)^{\text{th}}$ and $(i)^{\text{th}}$ samples using the conditions

$$\left| i_{\mathrm{P}}^{(k)} - i_{\mathrm{P}}^{(k-w_2)} \right| \le TH_1, \tag{11}$$

$$\left| i_{\mathrm{P}}^{(i)} - i_{\mathrm{P}}^{(i-w_2)} \right| \le TH_1, \tag{12}$$

where $w_2 \ll w_1$ is a short observation window to check that the measured values for i_p are transient-free and the battery operation has been stable when measuring those samples. The exact values of w_1 and w_2 are selected on a case-by-case basis according to battery parameters and operating conditions. However, simple tests can determine suitable ranges for w_1 as well as w_2. Initially, a second- or third-order RC circuit can approximate the voltage response of the battery to a current step with a relatively good accuracy during short intervals, e.g., few seconds. The suitable range of w_2 can be

$$w_2 \ge \frac{T_{\mathrm{settling}}}{T_S}, \tag{13}$$

where T_{settling} is the settling time of the voltage response with a 2% band. Additionally, TH_1 is the average amplitude of the current sensor noise. Additionally, the value of w_2 should be small enough that other states of the battery, particularly its SOC, can be assumed constant. Therefore, limiting the maximum possible variations of the SOC to 1%, the upper limit for the w_2 follows

TABLE II
PSEUDO-CODE OF THE DKF ESTIMATOR

1. Initialize $\boldsymbol{R}_{\mathbf{bt}}$, $\boldsymbol{V}_{\mathbf{bt}}$, $\boldsymbol{P}_{\mathbf{R}}^{+0}$, $\boldsymbol{P}_{\mathbf{V}}^{+0}$
2. Get new sample (k) **and** $i = k - w_1$
3. IF $\boldsymbol{S}_{\mathbf{U}}^{(k)} = \boldsymbol{S}_{\mathbf{U}}^{(k-w_1)}$ **&** $\boldsymbol{S}_{\mathbf{L}}^{(k)} = \boldsymbol{S}_{\mathbf{L}}^{(k-w_1)}$
↪ Go to step 4
ELSE
↪ $i = k - w_1 - 1$
↪ Repeat step 3
4. IF $\left|i_{\mathrm{P}}^{(k)} - i_{\mathrm{P}}^{(k-w_2)}\right| \& \left|i_{\mathrm{P}}^{(i)} - i_{\mathrm{P}}^{(i-w_2)}\right| \le TH_1$
IF $\left|i_P^{(k)} - i_P^{(i)}\right| \ge TH_2$ **&** $D^k == D^i$
↪ Update $\boldsymbol{R}_{\mathbf{bt}}$
↪ Update $\boldsymbol{V}_{\mathbf{OC}}$
ELSE
↪ Only update $\boldsymbol{V}_{\mathbf{OC}}$
ELSE
↪ Return to step 2
5. FOR $n \in [k - w_2, k]$
↪ $V_{\mathrm{est}}^{(n)} = \boldsymbol{S}_{\mathbf{U}} \boldsymbol{V}_{\mathbf{bt}} - (\boldsymbol{S}_{\mathbf{U}}(\boldsymbol{R}_{\mathbf{bt}} + \boldsymbol{R}_{\mathbf{sw}}) + \boldsymbol{S}_{\mathbf{L}}\boldsymbol{R}_{\mathbf{D}}) i_{\mathrm{p}}^{(k)}$
↪ $\overline{E_{\mathrm{v}}} = \overline{E_{\mathrm{v}}} + \frac{1}{w_1}|v_{\mathrm{est}}^{(n)} - v_{\mathrm{p}}^{(n)}|$
6. IF $\overline{E_{\mathrm{v}}} \le TH_3$
↪ Estimator is converged
ELSE
↪ $\boldsymbol{P}_{\mathbf{V}}^{+(k)} = \boldsymbol{P}_{\mathbf{V}}^{+(k)} + \frac{1}{w_1}|v_{\mathrm{est}}^{(k)} - v_{\mathrm{p}}^{(k)}|$
↪ $\boldsymbol{P}_{\mathbf{R}}^{+(k)} = \boldsymbol{P}_{\mathbf{R}}^{+(k)} + \frac{1}{w_1}|v_{\mathrm{est}}^{(k)} - v_{\mathrm{p}}^{(k)}|$
↪ Go to step 2

KF for $\boldsymbol{R}_{\mathbf{bt}}$:
↪ $\boldsymbol{P}_{\mathbf{R}}^{-(k)} = \boldsymbol{P}_{\mathbf{R}}^{+(k-1)} + \boldsymbol{Q}_{\mathbf{R}}$
↪ $\boldsymbol{K}_{\mathbf{R}} = \boldsymbol{P}_{\mathbf{R}}^{-(k)} \boldsymbol{S}_{\mathbf{U}} \left(\boldsymbol{S}_{\mathbf{U}} \boldsymbol{P}_{\mathbf{R}}^{-(k)} \boldsymbol{S}_{\mathbf{U}}^{T} + R_{\mathrm{R}}\right)^{-1}$
↪ $y_1 = -\frac{\Delta v_{\mathrm{p}}}{\Delta i_{\mathrm{p}}} - \boldsymbol{S}_{\mathbf{U}}\boldsymbol{R}_{\mathbf{sw}} - \boldsymbol{S}_{\mathbf{L}}\boldsymbol{R}_{\mathbf{D}}$
↪ $\hat{y}_1 = \boldsymbol{S}_{\mathbf{U}} \boldsymbol{R}_{\mathbf{bt}}^{(k-1)}$
↪ $\boldsymbol{R}_{\mathbf{bt}}^{(k)} = \boldsymbol{R}_{\mathbf{bt}}^{(k-1)} + \boldsymbol{K}_{\mathbf{R}}(y_1 - \hat{y}_1)$
↪ $\boldsymbol{P}_{\mathbf{R}}^{+(k)} = (\boldsymbol{I} - \boldsymbol{K}_{\mathbf{R}}\boldsymbol{S}_{\mathbf{U}})\boldsymbol{P}_{\mathbf{R}}^{-(k)}(\boldsymbol{I} - \boldsymbol{K}_{\mathbf{R}}\boldsymbol{S}_{\mathbf{U}})^T + \boldsymbol{K}_{\mathbf{R}} R_{\mathrm{R}} \boldsymbol{K}_{\mathbf{R}}^T$

KF for $\boldsymbol{V}_{\mathbf{OC}}$:
↪ $\boldsymbol{P}_{\mathbf{V}}^{-(k)} = \boldsymbol{P}_{\mathbf{V}}^{-(k-1)} + \boldsymbol{Q}_{\mathbf{V}}$
↪ $\boldsymbol{K}_{\mathbf{V}} = \boldsymbol{P}_{\mathbf{V}}^{-(k)} \boldsymbol{S}_{\mathbf{U}} \left(\boldsymbol{S}_{\mathbf{U}} \boldsymbol{P}_{\mathbf{V}}^{-(k)} \boldsymbol{S}_{\mathbf{U}}^{T} + R_{\mathrm{V}}\right)^{-1}$
↪ $y_2 = V_2 - \left(\boldsymbol{S}_{\mathbf{U}}\boldsymbol{R}_{\mathbf{bt}}^{(k)} - \boldsymbol{S}_{\mathbf{U}}\boldsymbol{R}_{\mathbf{sw}} - \boldsymbol{S}_{\mathbf{L}}\boldsymbol{R}_{\mathbf{D}}\right) I_2$
↪ $\hat{y}_2 = \boldsymbol{S}_{\mathbf{U}} \boldsymbol{V}_{\mathbf{bt}}^{(k-1)}$
↪ $\boldsymbol{V}_{\mathbf{bt}}^{(k)} = \boldsymbol{V}_{\mathbf{bt}}^{(k-1)} + \boldsymbol{K}_{\mathbf{V}}(y_2 - \hat{y}_2)$
↪ $\boldsymbol{P}_{\mathbf{V}}^{+(k)} = (\boldsymbol{I} - \boldsymbol{K}_{\mathbf{V}}\boldsymbol{S}_{\mathbf{U}})\boldsymbol{P}_{\mathbf{V}}^{-(k)}(\boldsymbol{I} - \boldsymbol{K}_{\mathbf{V}}\boldsymbol{S}_{\mathbf{U}})^T + \boldsymbol{K}_{\mathbf{V}} R_{\mathrm{V}} \boldsymbol{K}_{\mathbf{V}}^T$

$$t_{\max} < 0.01 \left(\frac{AH_{\mathrm{rated}}}{I_{\max}} \times 3600\right) \Rightarrow w_2 < \frac{t_{\max}}{T_{\mathrm{s}}}. \tag{14}$$

Next, the estimator checks the possibility of updating the internal resistance vector per

$$\left| i_{\mathrm{p}}^{(k)} - i_{\mathrm{p}}^{(i)} \right| \ge TH_2, \tag{14}$$

where TH_2 is the threshold that determines the minimum required current variation to update the internal resistance vector. Reducing the values of TH_2 will worsen the effect of measurement noise and increasing it can reduce how often $\boldsymbol{R}_{\boldsymbol{bt}}$ is updated. As a rule of thumb, $10\,TH_1 \le TH_2 \le 100\,TH_1$ can be selected.

Considering (14), the DKF algorithm updates the estimated internal resistance vector, as presented in Table II. First, the a-priori covariance matrix and the Kalman gain are updated per

$$\boldsymbol{P}_{\mathbf{R}}^{-(k)} = \boldsymbol{P}_{\mathbf{R}}^{+(k-1)} + \boldsymbol{Q}_{\mathbf{R}}, \tag{15}$$

$$\boldsymbol{K}_{\mathbf{R}} = \boldsymbol{P}_{\mathbf{R}}^{-(k)} \boldsymbol{S}_{\mathbf{U}} \left(\boldsymbol{S}_{\mathbf{U}} \boldsymbol{P}_{\mathbf{R}}^{-(k)} \boldsymbol{S}_{\mathbf{U}}^{T} + R_{\mathrm{R}}\right)^{-1}, \tag{16}$$

where $\boldsymbol{P}_{\mathbf{R}}^{-(k)}$ is the new priori covariance matrix and $\boldsymbol{Q}_{\mathbf{R}}$ is the covariance matrix of the process noise that characterizes modeling errors. Since the operation of each module is completely independent of other modules, the individual modeling noise/error for the modules is also independent. Additionally, the measurement and process noises are assumed independent, zero-mean, and white [46]. Therefore, $\boldsymbol{Q}_{\mathbf{R}}$ (and also $\boldsymbol{Q}_{\mathbf{V}}$) are defined as a diagonal matrix. The amplitude of the non-zero elements of $\boldsymbol{Q}_{\mathbf{R}}$ depend on the modeling accuracy and update rate of the algorithm. Additionally, R_{R} is a scalar that represents measurement noise.

The value of $\boldsymbol{Q}_{\mathbf{R}}$ can be fairly small and the value of R_{R} should be large to account for the observed switching noise. A small $\boldsymbol{Q}_{\mathbf{R}}$ and a large R_{R} is reasonable, since the internal resistance variations have relatively slow dynamics. The suitable $\boldsymbol{Q}_{\mathbf{R}}$ values can be selected heuristically [46]. Based on the nominal parameters of the battery, i.e., the values of $\boldsymbol{Q}_{\mathbf{R}}$ elements can be selected within the range of 2% to 5% of the battery model's accuracy

divided by the number of samples in one cycle of switching. Similarly, the value of R_R depends on measurement noise as well as the measurement resolution and should be determined heuristically, where $R_{\mathrm{R}} \geq \frac{f_s}{f_{sw}} \times \frac{Noise_V}{Noise_I}$ can serve as a good starting point. The ratio of $\frac{f_s}{f_{sw}}$ is the number of samples in one complete switching cycle.

Next, the vector of internal resistances is updated with the new measurements using

$$\boldsymbol{R}_{\mathbf{bt}}^{(\boldsymbol{k})} = \boldsymbol{R}_{\mathbf{bt}}^{(\boldsymbol{k-1})} + \boldsymbol{K}_{\mathbf{R}}(y_1 - \hat{y}_1), \tag{17}$$

where $\hat{y}_1$ and y_1 are measured and estimated equivalent resistance of the whole system as

$$y_1 = -\frac{\Delta v_{\mathrm{p}}}{\Delta i_{\mathrm{p}}}, \tag{18}$$

$$\hat{y}_1 = \boldsymbol{S}_{\mathbf{U}}\boldsymbol{R}_{\mathbf{bt}}^{(\boldsymbol{k-1})} - \boldsymbol{S}_{\mathbf{U}}\boldsymbol{R}_{\mathbf{sw}} - \boldsymbol{S}_{\mathbf{L}}\boldsymbol{R}_{\mathbf{D}}. \tag{19}$$

Lastly, the posterior covariance matrix ($\boldsymbol{P}_{\mathbf{R}}^{+(\boldsymbol{k})}$) is calculated using the updated $\boldsymbol{R}_{\mathbf{bt}}$ per

$$\boldsymbol{P}_{\mathbf{R}}^{+(\boldsymbol{k})} = (\boldsymbol{I} - \boldsymbol{K}_{\mathbf{R}}\boldsymbol{S}_{\mathbf{U}})\boldsymbol{P}_{\mathbf{R}}^{-(\boldsymbol{k})}(\boldsymbol{I} - \boldsymbol{K}_{\mathbf{R}}\boldsymbol{S}_{\mathbf{U}})^{\boldsymbol{T}} + \boldsymbol{K}_{\mathbf{R}}R_{\mathrm{R}}\boldsymbol{K}_{\mathbf{R}}^{\boldsymbol{T}}. \tag{20}$$

A similar procedure should be followed to update the vector of open-circuit voltages using the DKF as depicted in Table II. It should be noted that this step is performed regardless of whether the battery resistances are updated or not.

In the last step, the output voltage of the system is estimated for multiple samples (e.g., $[k - w_1, \dots, k]$) with the updated vectors per

$$v_{\mathrm{est}}^{(n)} = \boldsymbol{S}_{\mathbf{U}}\boldsymbol{V}_{\mathbf{bt}} - (\boldsymbol{S}_{\mathbf{U}}\boldsymbol{R}_{\mathbf{bt}} + \boldsymbol{S}_{\mathbf{U}}\boldsymbol{R}_{\mathbf{sw}} + \boldsymbol{S}_{\mathbf{L}}\boldsymbol{R}_{\mathbf{D}})i_{\mathrm{p}}^{(n)} \tag{21}$$

and compared with the measured values (e.g., $[v_{\mathrm{p}}^{(k-w_1)} \dots v_{\mathrm{p}}^{(k)}]$) to calculate the average error ($\overline{E_{\mathrm{v}}}$) using

$$\overline{E_{\mathrm{v}}} = \frac{1}{w_1}\sum_{n=k-w_1}^{k} |v_{\mathrm{est}}^{(n)} - v_{\mathrm{p}}^{(n)}|. \tag{22}$$

State estimation convergence of the KF algorithm is guaranteed, given that the system model is *detectable*. A well-established *detectability* analysis is based on the rank of matrix $[\mathbf{A}\ \mathbf{CA}\ \mathbf{CA}^2 \dots]^{\mathrm{T}}$. For both KF algorithms, this matrix can be obtained as $[\boldsymbol{I}\ \boldsymbol{S}_{\mathbf{U}}]^{\mathrm{T}}$, in which $\boldsymbol{I}$ is the identity. This matrix has full rank. Therefore, the system is *detectable* and has guaranteed convergence [47, 48].

When the estimators converge, the average error between the estimated and measured output voltage within our sliding window will be lower than a predetermined threshold (TH_3), e.g., $\overline{E_{\mathrm{v}}} < 1\%$. A $TH_3 = 1\%$ means that we consider the estimator converged only when the average error is below 1%. After the estimator is converged for the first time, the values of $\boldsymbol{P}_{\mathbf{R}}$ and $\boldsymbol{P}_{\mathbf{V}}$ are reduced and the parameters are only changed very slowly. While this feature reduces the noise sensitivity of the estimator to measurements, it can reduce the convergence speed in case of variation in the overall model of the system, e.g., due to fault occurrence. Therefore, each time $\overline{E_{\mathrm{v}}} > TH_3$, the term $\frac{1}{w_1}|v_{\mathrm{est}}^{(k)} - v_{\mathrm{p}}^{(k)}|$ is added to both $\boldsymbol{P}_{\mathbf{R}}$ and $\boldsymbol{P}_{\mathbf{V}}$.

The added terms to $\boldsymbol{P}_{\mathbf{R}}$ and $\boldsymbol{P}_{\mathbf{V}}$ when the estimation has diverged from the measurement in effect temporarily increase the $\boldsymbol{Q}_{\mathbf{R}}$ and $\boldsymbol{Q}_{\mathbf{V}}$. This would lead to improving the convergence speed as well as its likelihood [49, 50]. However, when the estimation gets close to the measurement, the added bias goes down, that reducing the Kalman filter sensitivity to noise and decreasing fluctuations around the convergence point. The adaptive learning rate can increase the convergence speed of the estimator [46].

C. Sequential Parameter Estimation and Conditions

To avoid well-known high-variability conditions with concurrent estimation of all degrees of freedom, the system separates the variables to be estimated during operation, and four operating modes with regard to the output current allow sequential estimation: *i*) zero current, *ii*) fast current variations, *iii*) gradual current variations, and iv) constant current.

When the system is idle with zero output current for a sufficiently long period, the internal chemical reactions of the battery would reach their equilibrium and the open-circuit voltage of the system can be estimated by directly measuring the terminal voltage of the battery [51]. Dependent on the application, such a condition usually occurs at least once in a day, for example when the EV is parked. In such situations, the controller can connect the modules in consecutive order and measure the steady-state change of the terminal voltage. While the estimation technique does not depend on this mode for convergence, it can still identify and compensate any bias or added offset due to switching operation.

According to (8), current variations are used to update the estimation of the internal resistances, which occur in the second and third modes. During rapid fluctuations of the current (e.g., 0.1 ~ 1 C/sec), the changes in SOC of the batteries are negligible (i.e., for a 1 C current, $\frac{\mathrm{d}\,SOC}{\mathrm{d}t} = 0.025\%$). On average, 0.025% variation in SOC leads to approximately 0.3 mV change in the open-circuit voltage. Hence, within the sliding window, the open-circuit voltage is stable (less than 1 mV variation) and any observed $\frac{\mathrm{d}V}{\mathrm{d}i}$ results merely from the internal resistance of the batteries and switches. However, gradual current variation (e.g., the variations that take more than a few seconds) with substantial dc component can change the SOCs of the batteries and therefore affect the output voltage of the system so that this situation is not advantageous for updating the internal resistances. Instead, when the current variations are gradual or the current is constant, the open-circuit voltages of the batteries can be updated. The variation threshold to differentiate between the gradual and rapid variation depends on the accuracy and noise rejection of the current and voltage sensor. The variation duration should be sufficiently higher than the main time constant (normally in the order of few milliseconds) of the battery and sufficiently low to avoid changes in the SOC or open-circuit voltage [28, 52]. Therefore, the duration threshold is selected to be one second.

The conditions required to update the estimates of the internal resistances of the batteries do not constrain the implementation of prognosis or monitoring functions and would not reduce the applicability of this method. Additionally, while the operation mode with gradual variations is not suitable to accurately estimate the internal resistances, it is still able to detect anomalies in the internal resistances and provide early warnings [20]. Since the variation of internal resistance of a battery due to battery aging is extremely slow (e.g., 2% per month according to [53]), large fluctuation in the estimated resistance of a module in a short period is a good indicator of faulty operation and/or fault placement [54, 55]. Fault detection and/or location is outside the focus of this paper.

The internal resistance of the battery can vary based on the SOC value as well as the battery temperature. However, the SOC variations are slow in comparison to the convergence speed of the estimator [29]. On the other hand, while the temperature dynamic

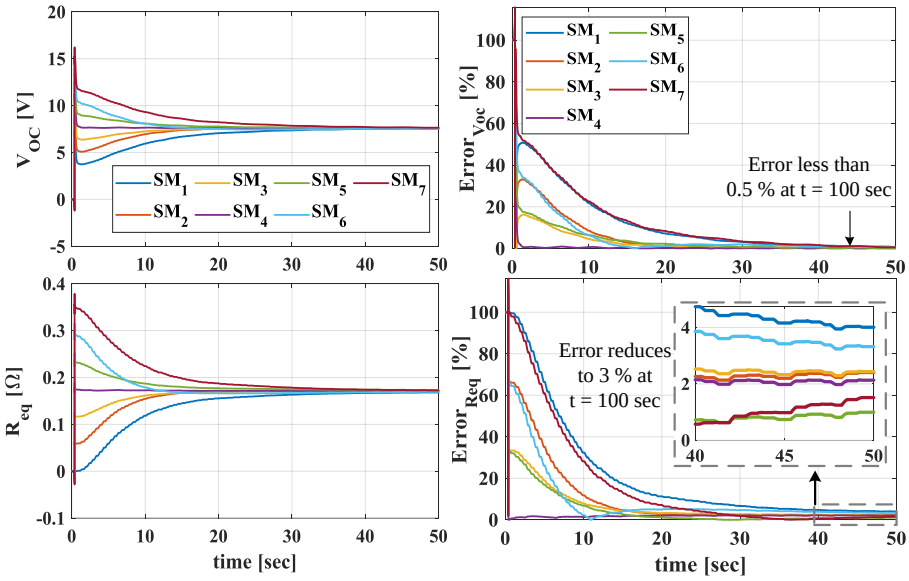

(a) (b)

Fig. 5. Simulation results for Scenario 1: (a) The estimated OCV and internal resistance of batteries, (b) the error between simulation results and ground-truth values

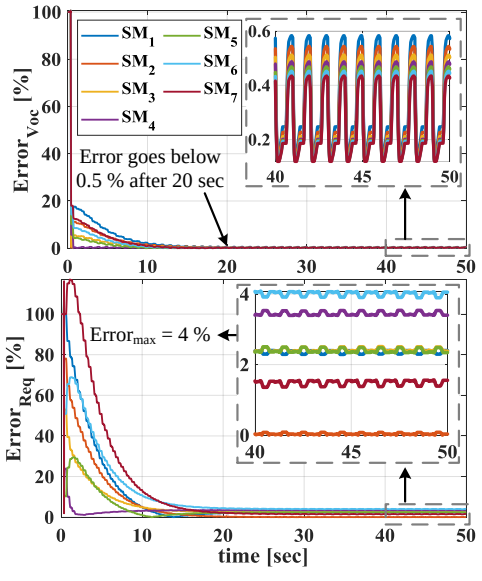

Fig. 7. Estimation errors in the second simulation scenario

is comparable to the convergence speed, the acquired internal resistance at other temperatures (e.g., at 20 °C) can be derived using a look-up table or a nonlinear function, for which methods are known in the literature [56, 57]. The look-up table or a nonlinear regression function for resistance, SOC, and temperature are generated on a case-by-case basis and are not the focus of this paper. Here, the temperature of the batteries is maintained at room temperature.

IV. Results and Discussion

To verify the robustness and precision of the developed estimator, three main scenarios are defined and applied for both the simulation model and the experimental setup. Two different systems are simulated; a low-power system model reflects the experimental setup in the lab, while a high-power model investigates the behavior of the estimator for scaled-up ratings.

A. Simulation Results

The performance and accuracy of the estimator are evaluated during balanced operation with relatively identical parameters as well as during imbalanced operation and/or with mismatched modules. Additionally, the effect of the modulation index on the accuracy of the system is investigated. Finally, the behavior of the estimator in a higher power system is also studied.

Table III provides the main parameters of both low- and high-power systems, with seven half-bridge modules. The parameters of the low-power system model the experimental setup. In the simulation, batteries are modeled using a simplified electrical equivalent circuit consisting of an internal resistance and a constant dc voltage source, as well as a second-order RC circuit [28]. The second-order RC circuit provides the dynamic response of the battery modules under load variations. Additionally, in all simulations, a uniform random noise is added to the output voltage and current with the amplitude of ± 0.2 %.

Fig. 5(a) presents the estimation results of OCV and internal resistance of the batteries for the first scenario. In Scenario 1, all the modules have identical parameters. The initial estimates for the OCVs are 2 V and for the internal resistances 0.05 Ω. The estimated values for the OCVs and internal resistances converge to the correct values for all seven modules in approximately 40 seconds. Additionally, Fig. 5(b) shows the absolute error for the OCVs and internal resistances, achieving less than 0.5% error for the voltages and a maximum 4.5% error for the resistances. The maximum fluctuation after convergence is 0.2%.

Scenario 2 investigates the behavior of the estimator for high-power applications, where the internal resistance of the batteries is considerably lower, such as in electric vehicles. Fig. 6 presents the graph of estimated and correct values for the voltage and resistance of each battery. Consequently, Fig. 7 presents the graphs of the error within this duration. Similar to Scenario 1, the estimator can easily identify the battery parameters with comparable errors. Similar to the previous scenario, the estimation error for the resistances stays below 4% and the maximum estimation error for the open-circuit voltages is less than 0.5%. The results demonstrate that the estimator converges in less than 20 seconds.

TABLE III
PARAMETERS OF THE SIMULATION AND EXPERIMENT TESTBENCH

PARAMETER	Low-Power Setup (experimental setup)	High-Power Setup (simulation study)
V_{dc}	30 – 40 V	500 – 600 V
C_{dc}	5 mF	5 mF
L_{dc}	1 mH	1 mH
R_{ldc}	0.05 Ω	0.05 mΩ
R_{load}	5 – 40 Ω	5 – 40 Ω
R_{ds}	1 mΩ	1 mΩ
R_{d}	1 mΩ	1 mΩ
$v_{oc,1-8}$	7.6 V	85 – 115 V
$r_{bt,1\sim8}$	0.18 Ω	18 mΩ
Scenario	1, 3	2

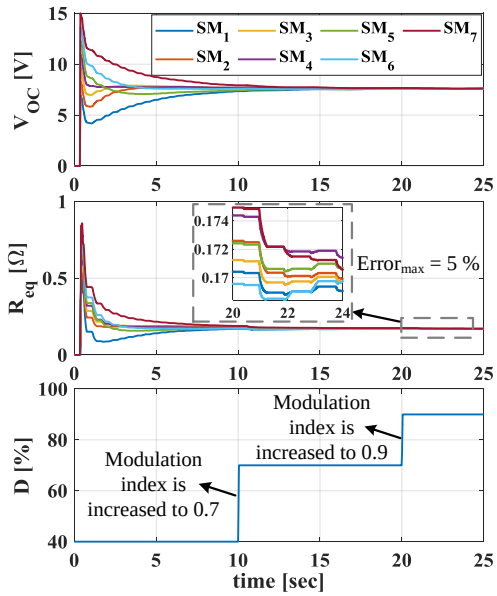

Fig. 8. The estimated OCVs, internal resistances, and duty cycle variations under the third simulation scenario

The third scenario investigates the effect of duty cycle variations on the estimator behavior. Fig. 8 presents the OCVs, internal resistances, and modulation index of the system under the third scenario. At $t = 10$ s, the modulation index is changed from 0.4 to 0.7; at $t = 20$ s, it steps from 0.7 to 0.9. The results show the gradual convergence of the estimation values to the ground truth, despite the varying duty cycle. Additionally, the speed of convergence slightly increases with this step, mainly because of the extra dynamics introduced to the system due to the modulation index variation.

B. Measurement Results

A prototype modular system with seven modules serves as an experimental proof of concept, as depicted in Fig. 9. The parameters of the prototype are identical to the low-power system tabulated in Table II.

The Li-ion battery connected to each module has a voltage ranging from 6.6 V to 8.3 V and consists of two sets of serial units, each unit having two parallel cells (2s 2p). Additionally, each module has a filtering capacitor, consisting of 2.2 mF electrolyte plus approximately 500 µF ceramic type. The current was measured using a current clamp with a 5 mA resolution. Two serial inductors provide the required inductance for the setup. Generic modules with Si-based field-effect transistors (FETs) allow for building the necessary power electronics circuit.

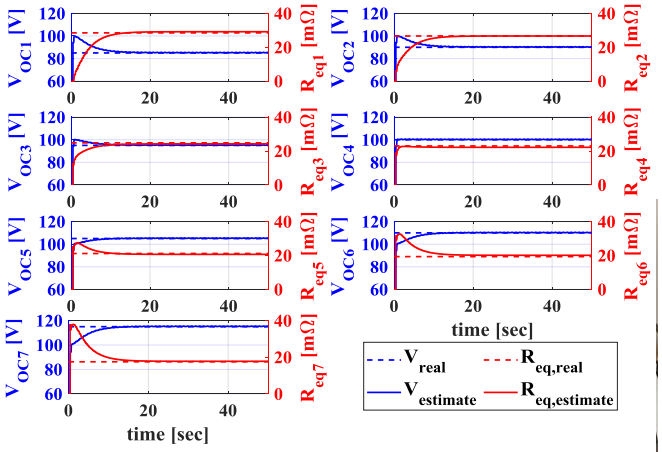

Fig. 6. The graph of the estimated parameters compared to ground-truth values in simulation of Scenario 2

The correct profile of the open-circuit voltage was obtained through measurement at extremely low discharge current ($\frac{1}{40}$C) as well as measuring the terminal voltage of the battery before and after the experiment. When at equilibrium, the terminal voltage of the battery is a good approximation of the open-circuit voltage. Hence, a 30-minute cool-down period before and after each experiment allows for the battery to achieve equilibrium and the open-circuit voltage of the battery to stabilize. The true profiles of the internal resistance of the batteries are separately derived through pulsed current with different SOCs and in multiple current amplitudes.

An FPGA-based sbRIO 9726 controller is responsible for the PSC modulation, the recording of the switching states, as well as the measured output current and voltage. The system is tested with switching rates ranging from 1 kHz to 5 kHz, and the sampling rate was selected to be 100 kHz, providing roughly 20 samples per cycle. The duration of each experiment is 50 seconds and at each time, the estimator starts with completely false values, to show that it can converge to correct ones.

Following the test procedure of the simulations, we evaluated the behavior of the system under varying conditions including different switching frequencies, different modulation indices with modules that have widely identical parameters or modules that are highly mismatched. The following presents a selected number of tests. Here, any current variations higher than 0.1 A/sec with a variation time of less than one second are considered to be rapid fluctuations and the suitable for updating the resistances.

Fig. 10(a) displays the OCVs and internal resistances of all modules in the normal conditions, where no obvious imbalance or mismatch exists among the modules. The modulation index is 0.5 and kept constant during the measurement. Although we introduced no intentional imbalance to the batteries and used similar battery modules, there are still small inherent differences between the modules. However, the estimator converges to the correct value for all seven modules. Additionally, the open-circuit voltage converges much faster, while the internal resistances are slower to converge. This phenomenon is mainly because of higher susceptibility to noise as well as less frequent updates in case of the resistance. Fig. 10(b) illustrates the measured output voltage of the system as well as the calculated output per (20) as the measurement continues and the estimations are updated. The small difference between the measured and calculated output voltage of the system mainly results from the switching noise, measurement bias, and dynamic differences that distorts the measurements.

Fig. 11 provides the estimation errors. The errors between the ground truth and corresponding estimations for OCVs and internal resistances are less than 1.5% and 5%, respectively. Although there is almost no straight way to tell the exact open-circuit voltage of a battery during operation, we measured the terminal voltage of the battery before and after the experiment when the current was zero. To allow for chemical reactions to reach equilibrium, the battery was kept under resting conditions (zero current at 20 °C) for at least four hours before and after the experiment when we measured the terminal voltages.

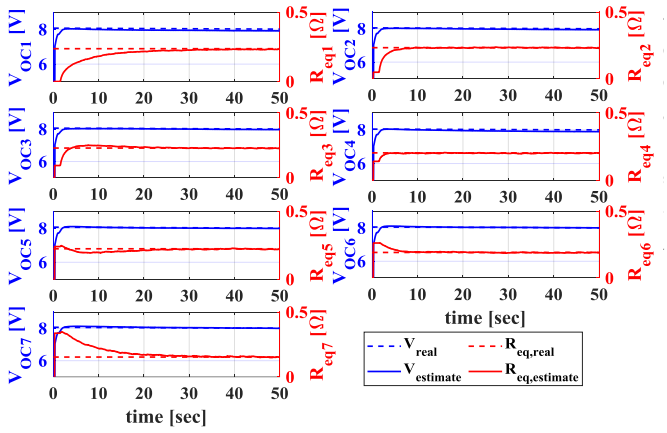

(a)

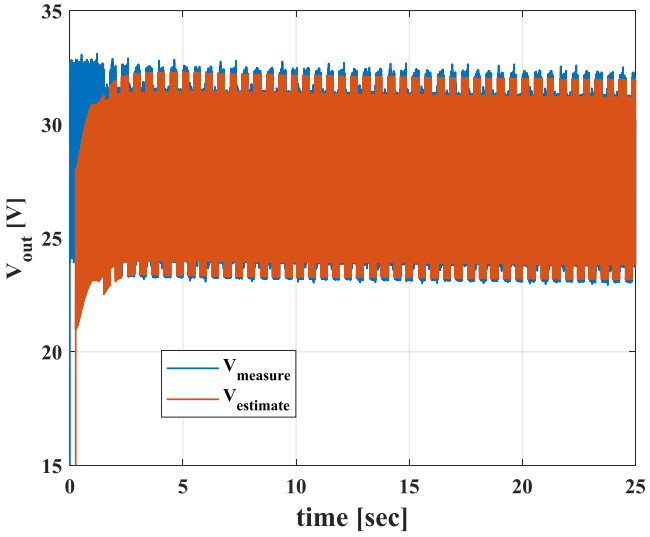

(b)

Fig. 10. Measurement Scenario 1: (a) The estimated OCV of all seven modules, (b) the estimated and measured output voltage

In the third scenario, the test is repeated for the situation in which the OCV of battery modules as well as internal resistances are different. Therefore, Module 7 is discharged, and a series resistance is added to Module 6. Furthermore, in this scenario, the modulation index of the system is changed to 0.75. Fig. 13(a) provides the estimation curves of open-circuit voltage and internal resistances as well as errors for this scenario. The initial estimation of the open-circuit voltages as well as the internal resistances are set to zero. However, even with large differences between the parameters of the modules and completely wrong initial values at the start, the estimator converges in approximately 35 seconds. The estimation error, as Fig. 13(b) shows, for the voltages is still below 1.5% and the estimation error for the internal resistance stays below 4.5%. Additionally, the maximum fluctuations around the convergence point are less than 1%.

In the proposed approach, the calculations of both KF algorithms are relatively light because each KF is formulated such that all non-diagonal entries of the system matrix will become zero, which makes the computations very light. Also, the computations regarding the output equation are simple scalar calculations. Therefore, the proposed algorithm contains only straightforward calculations at each iteration, which can be even precalculated to avoid large matrix-based computations. To verify this, we generated C code for a TMS320F28379D signal processor using MATLAB embedded coder and ran the algorithm with approximately 100 µs execution time for each complete iteration, i.e., 10 kHz iteration speed for the algorithm. Therefore, the algorithm can update the estimations every ten samples, assuming a 100 kHz sampling rate. Understandably, the autogenerated codes through MATLAB and the TI toolchain have a large overhead and much lower execution times are expected when the complete code is written in C directly and optimized.

V. Conclusion and Future Work

Whereas modular or reconfigurable energy storage systems offer many advantages, their need for a complex and expensive monitoring and control subsystem hinders their expansion in

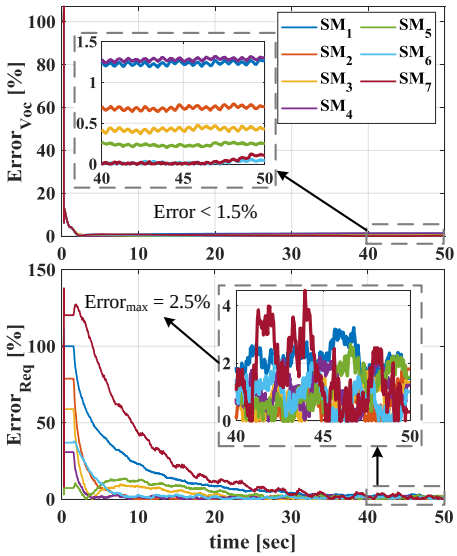

Fig. 11. Estimation errors of the measurement for Scenario 1

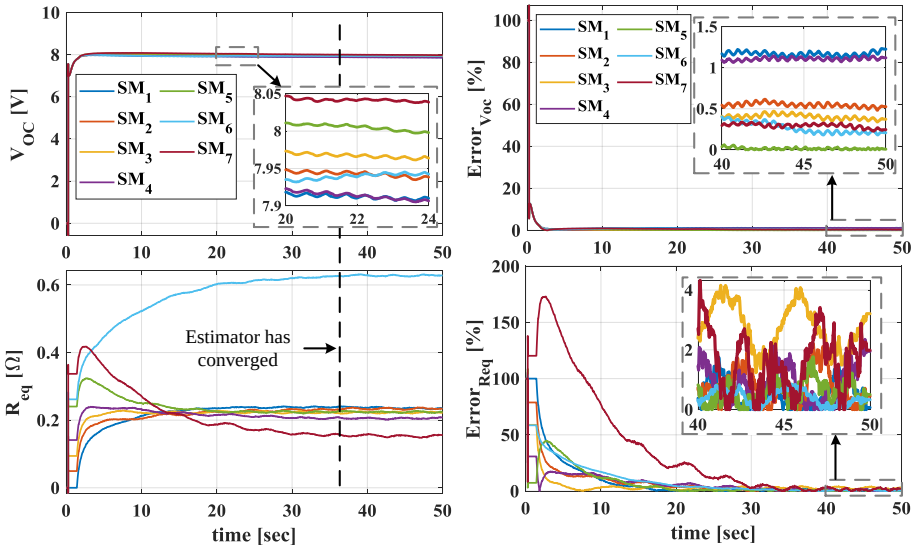

(a) (b)

Fig. 12. Measurement Scenario 2: (a) estimation results for Scenario 2, (b) estimation errors of Scenario 2

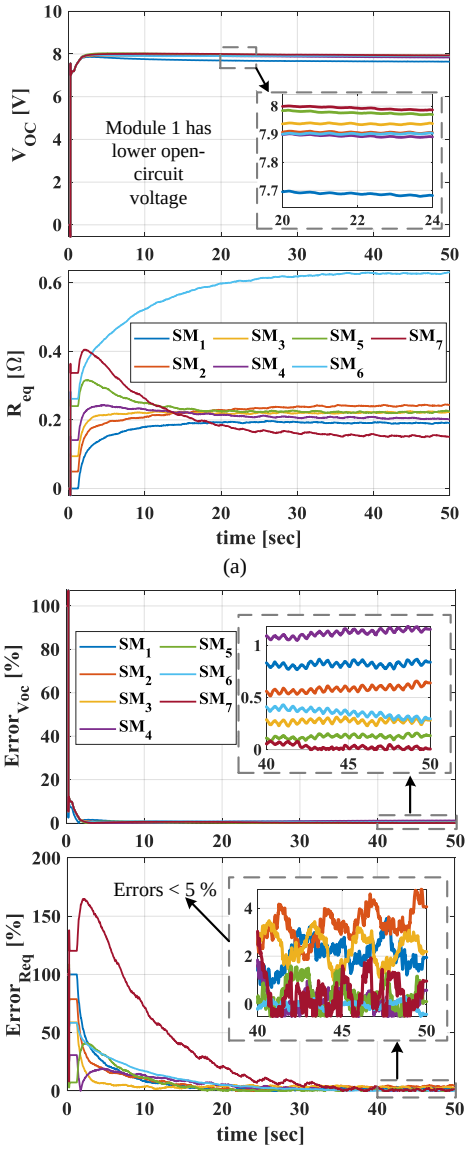

Fig. 13. Measurement Scenario 3: (a) estimation results for Scenario 3, (b) estimation errors of Scenario 3

many applications that are cost-sensitive or need a second source for sensor information for safety aspects, such as electromobility and its periphery. However, the existing estimation methods neglect important parameters, including the internal resistance of the battery. This paper fills the gap by presenting an estimation technique based on an adaptive DKF to estimate the equivalent internal resistance as well as the open-circuit voltage of all battery modules using only the voltage and current measurements at the output terminal of the system. These sensors are typically anyway present for system-level controllers [10].

The proposed estimation technique exploits the already available data about the output voltage and current of the pack as well as the switching states of the modules and can achieve accuracy levels of less than 1.5% and 5% for voltage and internal resistance, respectively. The proposed technique can reduce the size and cost of the monitoring circuit of a system with seven modules to less than one-eighth of its initial size, mainly through reducing the sensor requirements. Furthermore, the proposed estimation algorithm scales well and can thus be easily extended to systems with a large number of modules or strings.

The proposed method furthermore has low computational burden and complexity, which can readily be implemented on affordable low- and medium-range controllers. Additionally, the adopted DKF algorithm can effectively handle measurement noise and modeling uncertainties. However, other iteration-based methods can be also applied instead of the DKF method with the provided pseudo-code and flow chart. Furthermore, the paper considers half-bridge modules as the most popular topology and therefore all the relations are derived according to half-bridge topology. However, the provided procedure can be similarly followed for other module topologies, e.g., full-bridge [58, 59].

The focus of this work is to estimate the open-circuit and internal resistance of all battery modules online and with minimum number of sensors. As a future extension, the procedure and formalism might also be applicable for acute detection of failures, which also manifests in extremely rapid variations of estimated impedance as well as open-circuit voltage. For this, however, the method has to become substantially faster through simplification at the acceptable loss of accuracy so that additional research is needed. In addition, the decoupling technique proposed in this paper, could be adopted for other topologies (see the online supplement for an example); further research will be needed to understand this aspect clearly.

REFERENCES

[1] O. S. M. Abushafa, S. M. Gadoue, M. S. A. Dahidah, D. J. Atkinson, and P. Missailidis, "Capacitor Voltage Estimation Scheme With Reduced Number of Sensors for Modular Multilevel Converters," *IEEE Journal of Emerging and Selected Topics in Power Electronics,* vol. 6, no. 4, pp. 2086-2097, 2018.

[2] S. D. Arco and J. A. Suul, "Estimation of sub-module capacitor voltages in modular multilevel converters," presented at the 2013 15th European Conference on Power Electronics and Applications (EPE), 2-6 Sept. 2013, 2013.

[3] A. A. Taffese, E. d. Jong, S. D'Arco, and E. Tedeschi, "Online Parameter Adjustment Method for Arm Voltage Estimation of the Modular Multilevel Converter," *IEEE Transactions on Power Electronics,* vol. 34, no. 12, pp. 12491-12503, 2019.

[4] F. Rong, X. Gong, X. Li, and S. Huang, "A New Voltage Measure Method for MMC Based on Sample Delay Compensation," *IEEE Transactions on Power Electronics,* vol. 33, no. 7, pp. 5712-5723, 2018.

[5] N. Tashakor, M. Kilictas, J. Fang, and S. Goetz, "Switch-Clamped Modular Multilevel Converters with Sensorless Voltage Balancing Control," *IEEE Transactions on Industrial Electronics,* 2020.

[6] M. Priya, P. Ponnambalam, and K. Muralikumar, "Modular-multilevel converter topologies and applications – a review," *IET Power Electronics,* vol. 12, no. 2, pp. 170-183, 2019.

[7] J. Fang, F. Blaabjerg, S. Liu, and S. M. Goetz, "A Review of Multilevel Converters With Parallel Connectivity," *IEEE Transactions on Power Electronics,* vol. 36, no. 11, pp. 12468-12489, 2021.

[8] M. Abdelsalam, S. Tennakoon, H. Diab, and M. I. Marei, "An ADALINE based capacitor voltage estimation algorithm for modular multilevel converters," presented at the 2016 19th International Symposium on Electrical Apparatus and Technologies (SIELA), 29 May-1 June 2016, 2016.

[9] Z. Li, R. Lizana, Z. Yu, S. Sha, A. V. Peterchev, and S. Goetz, "A Modular Multilevel Series/Parallel Converter for Wide Frequency Range Operation," *IEEE Transactions on Power Electronics,* vol. 34, no. 10, pp. 9854-9865, 2019.

[10] S. M. Goetz, Z. Li, A. V. Peterchev, X. Liang, C. Zhang, and S. M. Lukic, "Sensorless scheduling of the modular multilevel series-parallel converter: enabling a flexible, efficient, modular battery," presented at the 2016 IEEE Applied Power Electronics Conference and Exposition (APEC), 2016.

[11] S. M. Goetz, Z. Li, X. Liang, C. Zhang, S. M. Lukic, and A. V. Peterchev, "Control of Modular Multilevel Converter With Parallel Connectivity—Application to Battery Systems," *IEEE Transactions on Power Electronics,* vol. 32, no. 11, pp. 8381-8392, 2017.

[12] Y. Li and Y. Han, "A Module-Integrated Distributed Battery Energy Storage and Management System," *IEEE Transactions on Power Electronics,* vol. 31, no. 12, pp. 8260-8270, 2016.
[13] N. Tashakor, E. Farjah, and T. Ghanbari, "A Bidirectional Battery Charger With Modular Integrated Charge Equalization Circuit," *IEEE Transactions on Power Electronics,* vol. 32, no. 3, pp. 2133-2145, 2017.
[14] G. L. Plett, "Extended Kalman filtering for battery management systems of LiPB-based HEV battery packs: Part 3. State and parameter estimation," *Journal of Power sources,* vol. 134, no. 2, pp. 277-292, 2004.
[15] S. Gonzalez, S. Verne, M. Valla, "Multilevel Converters for Industrial Applications," 2014.
[16] D. Ronanki and S. S. Williamson, "Modular multilevel converters for transportation electrification: Challenges and opportunities," *IEEE Transactions on Transportation Electrification,* vol. 4, no. 2, pp. 399-407, 2018.
[17] Z. Li, R. Lizana, S. Sha, Z. Yu, A. V. Peterchev, and S. Goetz, "Module Implementation and Modulation Strategy for Sensorless Balancing in Modular Multilevel Converters," *IEEE Transactions on Power Electronics,* 2018.
[18] N. Tashakor, F. Iraji, and S. G. Goetz, "Low-Frequency Scheduler for Optimal Conduction Loss in Series/Parallel Modular Multilevel Converters," *IEEE Transactions on Power Electronics,* in press, 2021.
[19] Z. Li, A. Yang, G. Chen, Z. Zeng, A. V. Peterchev, and S. M. Goetz, "A high-frequency pulsating dc link for electric vehicle drives with reduced losses," presented at the IEEE Industrial Electroncis Society (IECON), Toronto, 2021.
[20] X. Tan *et al.*, "Real-Time State-of-Health Estimation of Lithium-Ion Batteries Based on the Equivalent Internal Resistance," *IEEE Access,* vol. 8, pp. 56811-56822, 2020.
[21] R. O. NEMES, S. M. CIORNEI, R. Mircea, and C. MARTIS, "Parameters identification using experimental measurements for equivalent circuit Lithium-Ion cell models," presented at the 2019 11th International Symposium on Advanced Topics in Electrical Engineering (ATEE), 2019.
[22] Y. Yang, Q. Ye, L. J. Tung, M. Greenleaf, and H. Li, "Integrated Size and Energy Management Design of Battery Storage to Enhance Grid Integration of Large-Scale PV Power Plants," *IEEE Transactions on Industrial Electronics,* vol. 65, no. 1, pp. 394-402, 2018.
[23] N. Tashakor, V. Monteiro, T. Ghanbari, and E. Farjah, "An Improved Modular Charge Equalization Structure for Series Cascaded Battery," presented at the 2019 27th Iranian Conference on Electrical Engineering (ICEE), 30 April-2 May 2019, 2019.
[24] A. Ghazanfari and Y. A. I. Mohamed, "A Hierarchical Permutation Cyclic Coding Strategy for Sensorless Capacitor Voltage Balancing in Modular Multilevel Converters," *IEEE Journal of Emerging and Selected Topics in Power Electronics,* vol. 4, no. 2, pp. 576-588, 2016.
[25] G. Chen, H. Peng, R. Zeng, Y. Hu, and K. Ni, "A Fundamental Frequency Sorting Algorithm for Capacitor Voltage Balance of Modular Multilevel Converter With Low-Frequency Carrier Phase Shift Modulation," *IEEE Journal of Emerging and Selected Topics in Power Electronics,* vol. 6, no. 3, pp. 1595-1604, 2018.
[26] X. Hui, F. Yatao, and W. Yiying, "Review of equalizing methods for battery pack," presented at the Electrical Machines and Systems (ICEMS), 2014 17th International Conference on, 22-25 Oct. 2014, 2014.
[27] K. Wang, Y. Deng, H. Peng, G. Chen, G. Li, and X. He, "An Improved CPS-PWM Scheme-Based Voltage Balancing Strategy for MMC With Fundamental Frequency Sorting Algorithm," *IEEE Transactions on Industrial Electronics,* vol. 66, no. 3, pp. 2387-2397, 2019.
[28] B. Arabsalmanabadi, N. Tashakor, S. Goetz, and K. Al-Haddad, "Li-ion Battery Models and A Simplified Online Technique to Identify Parameters of Electric Equivalent Circuit Model for EV Applications," presented at the IECON 2020 The 46th Annual Conference of the IEEE Industrial Electronics Society, 18-21 Oct. 2020, 2020.
[29] J. Meng *et al.*, "An Overview and Comparison of Online Implementable SOC Estimation Methods for Lithium-ion Battery," *IEEE Transactions on Industry Applications,* vol. 54, no. 2, pp. 1583-1591, 2018.
[30] H. Givi, E. Hosseini, and E. Farjah, "Estimation of Batteries Voltages and Resistances in Modular Multilevel Converter With Half-Bridge Modules Using Modified PSO Algorithm," presented at the 2021 12th Power Electronics, Drive Systems, and Technologies Conference (PEDSTC), 2-4 Feb. 2021, 2021.
[31] S. D. Arco and J. A. Suul, "Estimation of sub-module capacitor voltages in modular multilevel converters," in *2013 15th European Conference on Power Electronics and Applications (EPE)*, 2013, pp. 1-10.
[32] B. G. Carkhuff, P. A. Demirev, and R. Srinivasan, "Impedance-Based Battery Management System for Safety Monitoring of Lithium-Ion Batteries," *IEEE Transactions on Industrial Electronics,* vol. 65, no. 8, pp. 6497-6504, 2018.
[33] M. D. Islam, R. Razzaghi, and B. Bahrani, "Arm-Sensorless Sub-Module Voltage Estimation and Balancing of Modular Multilevel Converters," *IEEE Transactions on Power Delivery,* vol. 35, no. 2, pp. 957-967, 2020.
[34] D. N. T. How, M. A. Hannan, M. S. H. Lipu, K. S. M. Sahari, P. J. Ker, and K. M. Muttaqi, "State-of-Charge Estimation of Li-Ion Battery in Electric Vehicles: A Deep Neural Network Approach," *IEEE Transactions on Industry Applications,* vol. 56, no. 5, pp. 5565-5574, 2020.
[35] G. Konstantinou, H. R. Wickramasinghe, C. D. Townsend, S. Ceballos, and J. Pou, "Estimation Methods and Sensor Reduction in Modular Multilevel Converters: A Review," presented at the 2018 8th International Conference on Power and Energy Systems (ICPES), 21-22 Dec. 2018, 2018.
[36] B. Arabsalmanabadi, N. Tashakor, A. Javadi, and K. Al-Haddad, "Charging Techniques in Lithium-Ion Battery Charger: Review and New Solution," presented at the IECON 2018 – 44th Annual Conference of the IEEE Industrial Electronics Society, 21-23 Oct. 2018, 2018.
[37] D. N. T. How, M. A. Hannan, M. S. H. Lipu, K. S. M. Sahari, P. J. Ker, and K. M. Muttaqi, "State-of-Charge Estimation of Li-ion Battery in Electric Vehicles: A Deep Neural Network Approach," *IEEE Transactions on Industry Applications,* in press, 2020.
[38] C. R. Gould, C. M. Bingham, D. A. Stone, and P. Bentley, "New Battery Model and State-of-Health Determination Through Subspace Parameter Estimation and State-Observer Techniques," *IEEE Transactions on Vehicular Technology,* vol. 58, no. 8, pp. 3905-3916, 2009.
[39] B. Arabsalmanabadi, N. Tashakor, Y. Zhang, K. Al-Haddad, and S. Goetz, "Parameter Estimation of Batteries in MMCs with Parallel Connectivity using PSO," presented at the IEEE Industrial Electroncis Society (IECON), Toronto, 2021.
[40] O. S. H. M. Abushafa, M. S. A. Dahidah, S. M. Gadoue, and D. J. Atkinson, "Submodule Voltage Estimation Scheme in Modular Multilevel Converters with Reduced Voltage Sensors Based on Kalman Filter Approach," *IEEE Transactions on Industrial Electronics,* vol. 65, no. 9, pp. 7025-7035, 2018.
[41] K. Bi, W. Yang, D. Xu, and W. Yan, "Dynamic SOC Balance Strategy for Modular Energy Storage System Based on Adaptive Droop Control," *IEEE Access,* vol. 8, pp. 41418-41431, 2020.
[42] Z. Ke *et al.*, "Capacitor Voltage Ripple Estimation and Optimal Sizing of Modular Multi-Level Converters for Variable-Speed Drives," *IEEE Transactions on Power Electronics,* vol. 35, no. 11, pp. 12544-12554, 2020.
[43] L. Lu, X. Han, J. Li, J. Hua, and M. Ouyang, "A review on the key issues for lithium-ion battery management in electric vehicles," *Journal of Power Sources,* vol. 226, pp. 272-288, 2013.
[44] B. Novakovic and A. Nasiri, "Modular Multilevel Converter for Wind Energy Storage Applications," *IEEE Transactions on Industrial Electronics,* vol. 64, no. 11, pp. 8867-8876, 2017.
[45] N. Tashakor, Z. Li, and S. M. Goetz, "A Generic Scheduling Algorithm for Low-Frequency Switching in Modular Multilevel Converters with Parallel Functionality," *IEEE Transactions on Power Electronics,* in press, 2020.
[46] S. D. Brown and S. C. Rutan, "Adaptive Kalman filtering," *Journal of Research of the National Bureau of Standards,* vol. 90, no. 6, p. 403, 1985.
[47] F. Naseri, E. Farjah, T. Ghanbari, Z. Kazemi, E. Schaltz, and J.-L. Schanen, "Online parameter estimation for supercapacitor state-of-energy and state-of-health determination in vehicular applications," *IEEE Transactions on Industrial Electronics,* vol. 67, no. 9, pp. 7963-7972, 2019.
[48] B. D. Anderson and J. B. Moore, *Optimal filtering*. Courier Corporation, 2012.
[49] O. Abushafa, S. Gadoue, M. Dhaidah, and D. Aktinson, "Capacitor voltage estimation in modular multilevel converters using a Kalman filter algorithm," presented at the 2015 IEEE International Conference on Industrial Technology (ICIT), 2015.
[50] J. Samantaray, R. Chakraborty, S. Chakrabarty, and A. Dey, "Discrete Time Adaptive Observation of Capacitor Voltage of Modular Multilevel Converters," presented at the 2020 IEEE 17th India Council International Conference (INDICON), 10-13 Dec. 2020, 2020.
[51] J. Meng, D. Stroe, M. Ricco, G. Luo, and R. Teodorescu, "A Simplified Model-Based State-of-Charge Estimation Approach for Lithium-Ion Battery With Dynamic Linear Model," *IEEE Transactions on Industrial Electronics,* vol. 66, no. 10, pp. 7717-7727, 2019.
[52] H. He, R. Xiong, X. Zhang, F. Sun, and J. Fan, "State-of-charge estimation of the lithium-ion battery using an adaptive extended Kalman filter based on an improved Thevenin model," *IEEE Transactions on vehicular technology,* vol. 60, no. 4, pp. 1461-1469, 2011.
[53] D. Stroe, M. Swierczynski, S. K. Kær, and R. Teodorescu, "Degradation Behavior of Lithium-Ion Batteries During Calendar Ageing—The Case of

the Internal Resistance Increase," *IEEE Transactions on Industry Applications,* vol. 54, no. 1, pp. 517-525, 2018.

[54] Y. Zheng, Y. Lu, W. Gao, X. Han, X. Feng, and M. Ouyang, "Micro-Short-Circuit Cell Fault Identification Method for Lithium-Ion Battery Packs Based on Mutual Information," *IEEE Transactions on Industrial Electronics,* vol. 68, no. 5, pp. 4373-4381, 2020.

[55] M. Seo, M. Park, Y. Song, and S. W. Kim, "Online detection of soft internal short circuit in lithium-ion batteries at various standard charging ranges," *IEEE Access,* vol. 8, pp. 70947-70959, 2020.

[56] L. C. Casals, A. M. S. González, B. A. García, and J. Llorca, "PHEV battery aging study using voltage recovery and internal resistance from onboard data," *IEEE Transactions on Vehicular Technology,* vol. 65, no. 6, pp. 4209-4216, 2015.

[57] A. Lievre, A. Sari, P. Venet, A. Hijazi, M. Ouattara-Brigaudet, and S. Pelissier, "Practical online estimation of lithium-ion battery apparent series resistance for mild hybrid vehicles," *IEEE Transactions on Vehicular Technology,* vol. 65, no. 6, pp. 4505-4511, 2015.

[58] G. Farivar, V. G. Agelidis, and B. Hredzak, "A generalized capacitors voltage estimation scheme for multilevel converters," presented at the 2014 16th European Conference on Power Electronics and Applications, 26-28 Aug. 2014, 2014.

[59] S. M. Goetz, A. V. Peterchev, and T. Weyh, "Modular Multilevel Converter With Series and Parallel Module Connectivity: Topology and Control," *Power Electronics, IEEE Transactions on,* vol. 30, no. 1, pp. 203-215, 2015.

Supplement I: Intuitive Illustration of a Dynamically Reconfigurable Battery

Fig. S1 provides an intuitive representation of dynamic reconfiguration of a modular battery. In Fig. S1(a), Module 2 is connected in series and discharging, whereas it is bypassed in Fig. S1(b). Continuous change of connection modes of modules (controlled by the PSC modulation) changes the equivalent electrical circuit of the system that renders the conventional state estimation techniques useless.

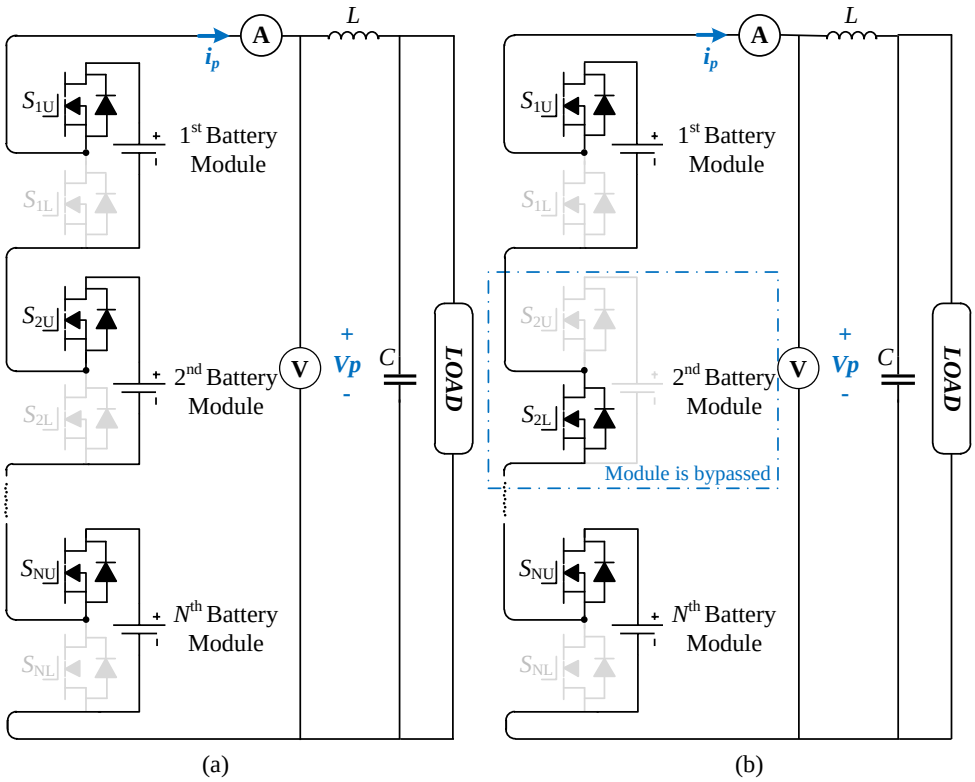

Fig. S1. Intuitive representation of a dynamic reconfiguration of a modular battery: (a) all modules are connected in series; (b) the second module is bypassed

Supplement II: Flowchart of the Proposed Adaptive Dual Kalman Filter

Fig. S2 shows the flowchart of the proposed dual KF estimation method. The controller records the output voltage and current samples as well as the switching states of the modules with two sliding windows each with w_2 sample depth, where the windows are w_1 samples apart from each other. These two sliding windows will be used by the controller to detect the operation mode of the system as discussed in Section III-B to determine which of the parameters can be updated. If the controller receives identical switching states and detects a variation in current, the controller will update the previous estimate of the internal resistance vector according to (17), otherwise, this step is skipped. Subsequently, the controller updates the vector of open-circuit voltages (see Table II) and returns to the beginning of the algorithm. When the average error between the estimation and measured value of the output voltage is below a certain threshold, then we can conclude that the estimator has converged to its final values.

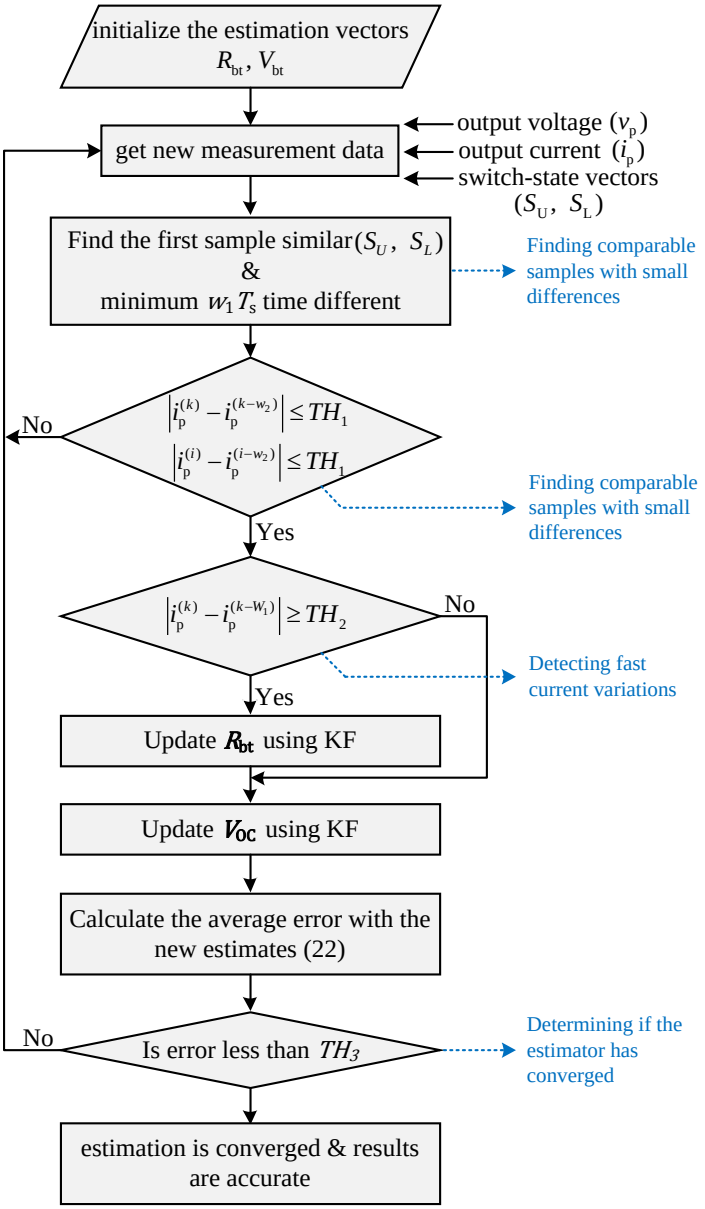

Fig. S2 The flowchart of the proposed DKF algorithm

Supplement III: Additional Compatible Topologies

Although the main analysis and results are provided for the half-bridge topology without considering a filter, the presented method can be further applied to other modular converters and reconfigurable battery systems, such as cascaded DC converters or half-bridge topologies with low-pass filters between battery and the half-bridge, which further adds to the appeal of the method[1]. As an example, Fig. S3 depicts a system, where an LC low-pass filter is placed between the half-bridge and the battery [2]. Additional filters in the module, reduce the dynamic response of the module to load change, which must be taken into account (use larger windows) in determining the suitable window sizes (w_1 and w_2). Additionally, the internal resistance of the inductance must be deducted from the final estimation per

$$\boldsymbol{R'_{bt}} = \boldsymbol{R_{bt}} - r_{\mathrm{int},L}. \tag{S1}$$

For verification, we have repeated the first scenario in a system with low-pass LC filters between the batteries and the half-bridges. All the parameters of the system remain constant, and the added L_f and C_f components were 10 µH and 20 µF, respectively. The internal resistance of the inductors ($r_{\mathrm{int},L}$) was 2 mΩ. In the following, the estimation results under these conditions are shown:

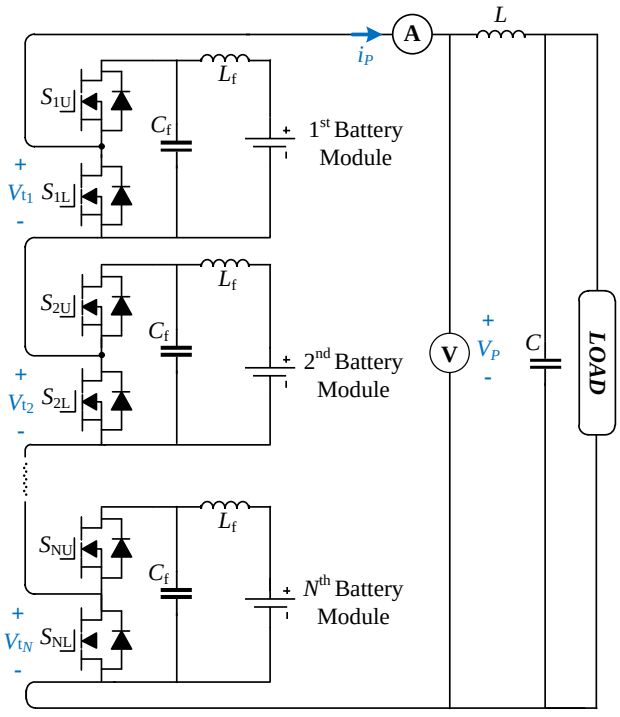

Fig. S3. Topology of the half-bridge modules with LC filter

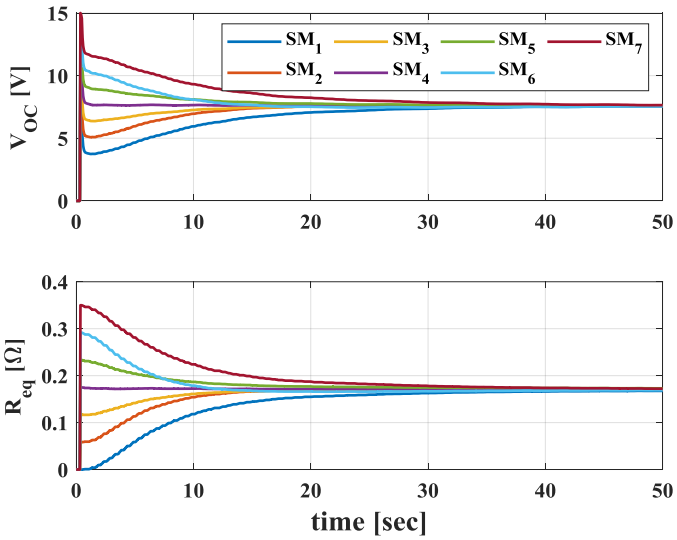

Fig. S4. Estimation results for the open-circuit voltage and internal resistances

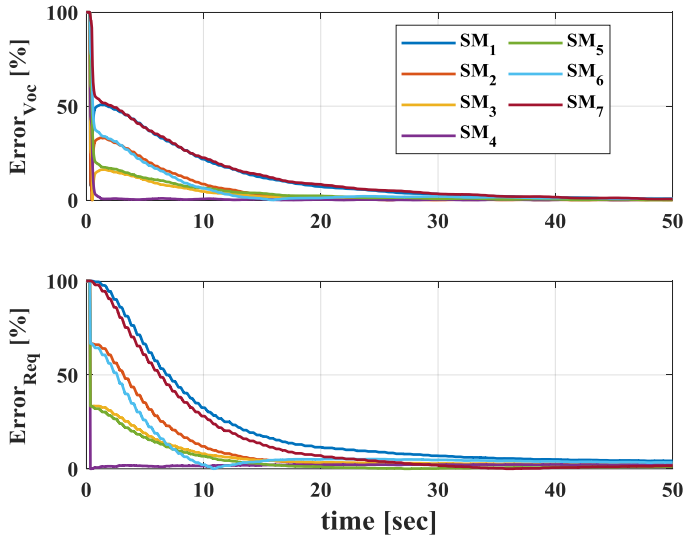

Fig. S5. Estimation errors for the open-circuit voltages and resistances

References

Note: This list contains only the references of the online supplement.

[1] N. Tashakor, E. Farjah, and T. Ghanbari, "A Bidirectional Battery Charger With Modular Integrated Charge Equalization Circuit," *IEEE Transactions on Power Electronics*, vol. 32, no. 3, pp. 2133-2145, 2017.

[2] B. Novakovic, and A. Nasiri, "Modular Multilevel Converter for Wind Energy Storage Applications," *IEEE Transactions on Industrial Electronics*, vol. 64, no. 11, pp. 8867-8876, 2017.